Nanoscale Research Letters

NANO EXPRESS Open Access

Efficient TiO_2 Surface Treatment Using Cs_2CO_3 for Solution-Processed Planar-Type Sb_2S_3 Solar Cells

Wook Hyun Kim†, Sungho Woo*†, Kang-Pil Kim, Soo-Min Kwon and Dae-Hwan Kim

Abstract

We report a highly effective surface treatment method for planar-type Sb_2S_3 solar cells by employing a Cs_2CO_3-modified compact TiO_2 (c-TiO_2) electron transport layer. It is found that surface treatment using a Cs_2CO_3 solution can shift the work function of c-TiO_2 upward and reduce its surface roughness. As a result, compared with the power conversion efficiency of untreated solar cells, that of the treated solar cells with a glass/FTO/c-TiO_2(/Cs_2CO_3)/Sb_2S_3/P3HT/Au structure significantly improved from 2.83 to 3.97%. This study demonstrates that the introduction of Cs_2CO_3 on a c-TiO_2 layer is a simple and efficient way to adjust the work function of the electron transport layer and fabricate high-performance planar-type Sb_2S_3 solar cells.

Keywords: Planar-type Sb_2S_3 solar cell, Electron transport layer, Surface treatment, Solution process, Cs_2CO_3

Background

Recently, many inorganic metal chalcogenides based on earth-abundant elements such as copper zinc tin selenide (CZTS), lead sulfide (PbS), copper (I) sulfide (Cu_2S), tin sulfide (SnS), and antimony sulfide (Sb_2S_3) have been investigated as absorber materials in low-cost thin film solar cells in order to replace the mainstream solution-processible absorbers such as copper indium gallium selenide (CIGS) and cadmium telluride (CdTe) [1]. However, the use of CZTS and PbS in the industry has severe drawbacks, because CZTS uses the toxic and harmful hydrazine (N_2H_4) and requires the complex control of multi-compound [2] and PbS contains Pb, which is also toxic and hazardous. Other potential materials such as Cu_2S and SnS have relatively low efficiencies compared to those of CIGS and CdTe. Sb_2S_3, however, has attracted attention as a candidate material due to its suitable band gap (~ 1.65 eV) and high absorption coefficient (> 10^5 cm^{-1}) for efficient light absorption, high dielectric constant for exciton dissociation, and good band alignment with various hole transport layers (HTLs) for efficient charge carrier transfer, in addition to its cost effectiveness, low toxicity, and excellent air stability [3–6].

There are two types of Sb_2S_3 solar cells based on the device structures: sensitized solar cell or planar-type solar cell. Sensitized solar cells originated from dye-sensitized solar cells (DSSCs) and have a F-doped tin oxide (FTO)/compact TiO_2 (c-TiO_2)/mesoporous TiO_2 (m-TiO_2)/Sb_2S_3/HTL/Au structure, while planar-type solar cells have a FTO/c-TiO_2/Sb_2S_3/HTL/Au structure [7].

In terms of device efficiency, sensitized Sb_2S_3 solar cells have a higher value than planar types due to their enhanced light-absorbing interfacial area owing to the m-TiO_2 structure. The factor that decides the performance of sensitized solar cells is their interface quality inside the device where charge carrier separation and transfer occur. Therefore, significant effort has been devoted to the optimization of the interfacial properties, including those of the m-TiO_2/Sb_2S_3 interface, Sb_2S_3/HTL interface, and HTL material itself [8]. Various kinds of HTL materials, such as 2,2′,7,7′-tetrakis[N,N-di(4--methoxyphenyl)amine]-9,9′-spirobifluorene

* Correspondence: shwoo@dgist.ac.kr
†Wook Hyun Kim and Sungho Woo contributed equally to this work.
Convergence Research Center for Solar Energy, Daegu Gyeongbuk Institute of Science and Technology (DGIST), Daegu 42988, Republic of Korea

(Spiro-OMeTAD) [9]; CuSCN, an inorganic p-type material [10]; poly(3-hexylthiophene) (P3HT), a conducting polymer [11]; and poly(2,6-(4,4-bis-(2-ethylhexyl)-4H-cyclopenta [2,1-b,3,4-b′]dithiophene)-alt-4,7(2,1,3-benzothiadiazole)) (PCPDTBT), a newly developed conjugated polymer [12], have been applied to adjust the Sb_2S_3/HTL interface and hole transport properties leading to a high fill factor (FF) and increased short-circuit current density (J_{SC}).

Several studies that focus on the improvement of the m-TiO_2/Sb_2S_3 interface properties have been also reported. Tsujimoto et al. modified the m-TiO_2 surface using Mg^{2+}, Ba^{2+}, and Al^{3+}, which effectively increase the power conversion efficiency (PCE) of all inorganic Sb_2S_3 solar cells that have the FTO/c-TiO_2/m-TiO_2/Sb_2S_3/CuSCN/Au structure [13]. Lan et al. used Li-doped m-TiO_2 to enhance the electron transport properties and change the Fermi energy level [14]. Fukumoto et al. reported the surface treatment of the Sb_2S_3/HTL interface using 1-decylphosphonic acid (DPA), which can be attached to both an uncovered m-TiO_2 surface and Sb_2S_3 surface to reduce recombination and increase the open-circuit voltage (V_{OC}) and FF [15].

In planar-type solar cells, in contrast to sensitized ones, charge carrier transport depends on the carrier mobility and diffusion length within the Sb_2S_3 layer, which are strongly correlated with the morphology, grain size, and crystallinity of the layer. Hence, most research on planar-type solar cells has been focused on improving the Sb_2S_3 thin film quality to achieve a large grain size and a high crystallinity by using various deposition techniques. For example, conventional chemical bath deposition (CBD) [16], thermal evaporation (TE) [17], rapid thermal evaporation (RTE) [18, 19], atomic layer deposition (ALD) [20], and nanoparticle ink coating [21] have been applied to fabricate Sb_2S_3 thin films. Recently, Wang et al. reported a fast chemical approach (FCA) that can be used to generate very large grain sizes via a one-step spin-coating process and subsequent annealing process using a butyldithiocarbamic acid (BDCA)-based metal-organic precursor solution [22]. Many types of metal oxides or hydroxides can be dissolved in BDCA, which is relatively nontoxic, inexpensive, and thermally degradable, and can be easily synthesized via the reaction of 1-butylamine ($CH_3(CH_2)_3NH_2$) and carbon disulfide (CS_2) [23].

Although the sensitized solar cells have a higher PCE (3–7.5%) than planar-type ones (2.5–5.8%), their device structure and fabrication process are complicated. Moreover, they contain a high degree of interface defects. A planar-type Sb_2S_3 device would have more potential for use in industrial-scale solar cells with a high efficiency and low cost, because it is conceptually simpler and easier to scale up and it is highly reproducible [24, 25].

Here, we report the surface treatment of a c-TiO_2 layer using Cs_2CO_3 solution to enhance the performance of planar-type Sb_2S_3 solar cells. The Sb_2S_3 layer was deposited via a simple FCA spin-coating process to realize a large grain size, which was previously reported by Wang et al.

Cs_2CO_3 has been widely studied for application in organic photovoltaics (OPV) [26–28], organic light-emitting devices (OLEDs) [29], and perovskite solar cells (PSCs) [30, 31] to improve electron transport due to its low-work function property. Although Cs_2CO_3 is usually decomposed at 550–600 °C, Liao et al. reported that Cs_2CO_3 can be decomposed into low-work function cesium oxide via a low-temperature (150–170 °C) thermal annealing process [26]. However, to the best of our knowledge, there is no study on the application of Cs_2CO_3 to Sb_2S_3 solar cells.

Surface treatment using Cs_2CO_3 can not only reduce the energy barrier by changing the work function of c-TiO_2, but also reduce the series resistance of the device by reducing the surface roughness of c-TiO_2. The treatment resulted in improved device parameters such as the V_{OC}, J_{SC}, and FF, and the PCE increased from 2.83 to 3.97%. We believe that this surface treatment of c-TiO_2 using Cs_2CO_3 solution can provide a simple and effective way of improving device performance in planar-type inorganic metal chalcogenide solar cells.

Methods/Experimental

Materials Used and Synthesis of Sb Complex

Antimony (III) oxide (Sb_2O_3, 99.99%), CS_2 (> 99.9%), n-butylamine ($CH_3(CH_2)_3NH_2$, n-BA, 99.5%), cesium carbonate (Cs_2CO_3, 99.9%), 2-methoxyethanol ($CH_3OCH_2CH_2OH$, 99.8%), titanium (IV) isopropoxide ($Ti(OCH(CH_3)_2)_4$, TTIP, 97%), poly(3-hexylthiophene) (P3HT, Mw 50–70K, regioregularity 91–94%, Rieke Metals), 1,2-dichlorobenzene (o-DCB, 99%), and ethanol (CH_3CH_2OH, anhydrous) were purchased from Sigma-Aldrich Co. and were used as received without further purification.

The Sb complex was synthesized according to a reported method [22]. Sb_2O_3 (1.0 mmol) was mixed with a solution of ethanol (2.0 mL) and CS_2 (1.5 mL) with magnetic stirring at room temperature. Then, n-butylamine (2.0 mL) was added to the solution slowly under continued stirring for at least 30 min to obtain a homogenous solution of antimony butyldithiocarbamates ($Sb(S_2CNHC_4H_9)_3$). Afterwards, 2 mL of this solution was diluted with 1 mL ethanol to form the Sb complex.

Device Fabrication

The planar-type Sb_2S_3 solar cells in this study have a typical structure of FTO/c-TiO_2/Sb_2S_3/P3HT/Au, where P3HT is employed as the HTL. The c-TiO_2 layer was deposited onto a cleaned FTO surface by spin-coating a mixed solution of 2 mL TTIP, 60 mL ethanol, 0.225 mL distilled water, and 0.03 mL HNO_3 at 3000 rpm for 30 s, followed by annealing at 500 °C for 60 min in air.

For surface modification using Cs_2CO_3, Cs_2CO_3 dissolved in a $CH_3OCH_2CH_2OH$ solution with certain concentrations (1, 3, 5, and 10 mg/mL) was spin-coated on a 10-min UV-ozone treated c-TiO_2 layer at 6000 rpm for 45 s. The films were then heat-treated at 150 °C for 10 min before the Sb_2S_3 layer was spin-coated.

For the Sb_2S_3 thin films, the Sb complex solution was spin-coated at a speed of 6000 rpm for 30 s, after which the films were annealed on a N_2-purged hot plate at 200 °C for 1 min and 350 °C for 2 min.

P3HT solution (10 mg in 1 mL o-DCB) was spin-coated on the Sb_2S_3/c-TiO_2/FTO substrate at a speed of 3000 rpm for 60 s, which was then heated on a hot plate at 100 °C for 30 min in air. Finally, the Au counter electrode was deposited using a thermal evaporator under a pressure of 5.0×10^{-6} Torr. Each device had an active area of 0.16 cm^2.

Measurement and Analysis

The surface and cross-sections of the Sb_2S_3 thin films were characterized using field-emission scanning electron microscopy (FE-SEM, S-4800, Hitachi). The surface morphology was studied using atomic force microscopy (AFM, Park NX10, Park Systems). The optical properties of c-TiO_2 were determined using a UV-Vis (Lambda 750, Perkin Elmer). The current density–voltage (J–V) characteristics were determined using a specialized solar cell measurement system equipped with an electrometer (model 2400, Keithley) and solar simulator (91192, Newport) with a 1-kW Xenon arc lamp (Oriel). The light intensity was adjusted to one sun (100 mW/cm^2) under AM 1.5G solar irradiation conditions using a radiant power energy meter (model 70260, Oriel). The series resistance (R_S) and shunt resistance (R_{SH}) were calculated from the slope of the corresponding J–V curves beyond V_{OC} and J_{SC}, respectively. The external quantum efficiency (EQE) was measured by a QuantX-300 quantum efficiency measurement system (Newport) equipped with a 100 W Xenon lamp. The structural information of FTO/c-TiO_2(/Cs_2CO_3) sample was characterized by multi-purpose X-ray diffraction (XRD) system (Empyrean, PANalytical) with θ-2θ mode at a scan rate of 0.05°/sec. The electronic state and energy level were analyzed using X-ray photoelectron spectroscopy (XPS) and ultraviolet photoelectron spectroscopy (UPS) in an ultrahigh vacuum environment (ESCALAB 250Xi, Thermo Scientific). UPS and XPS spectra were obtained by using the He I line (hν = 21.2 eV) and the Al Kα radiation source (hν = 1486.6 eV), respectively. The XPS depth profiling was obtained using Ar^+-cluster ion gun and etch rate of 1 Å/sec.

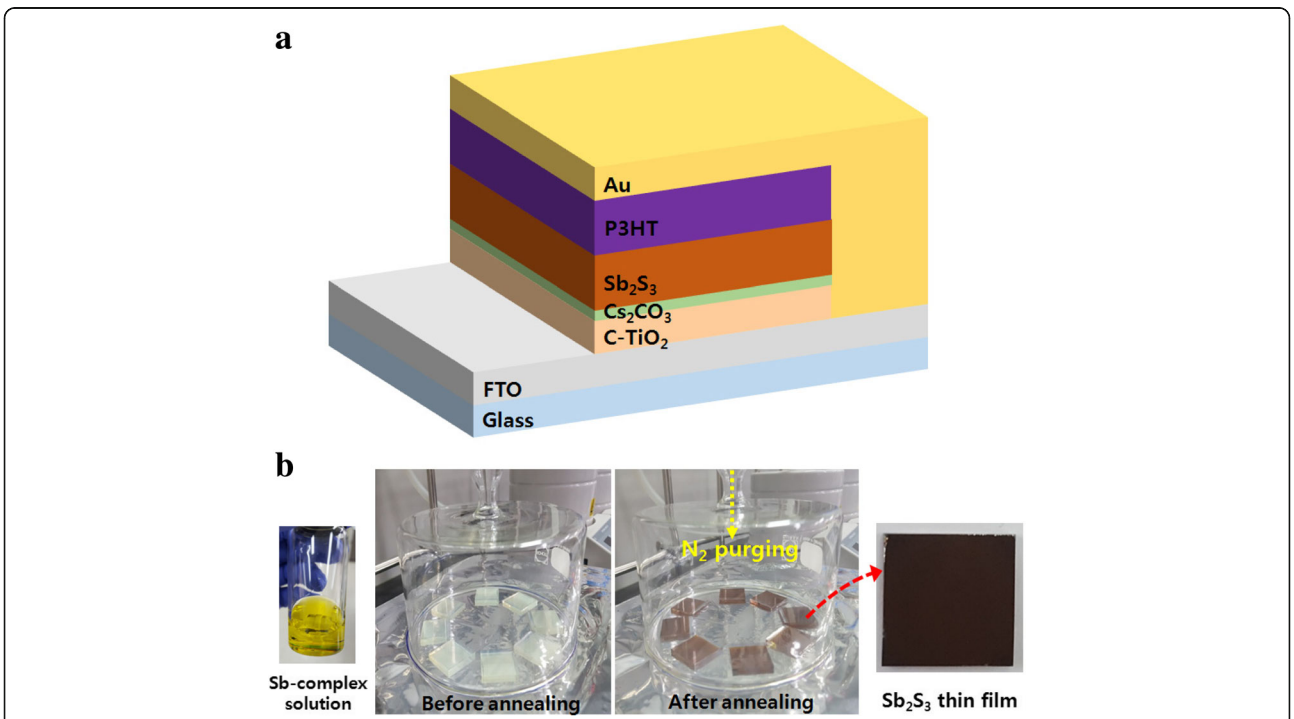

Fig. 1 **a** Schematic of the device structure of planar-type Sb_2S_3 solar cells. **b** Sb_2S_3 thin film fabrication process using FCA method

Results and Discussion

Figure 1a shows a schematic of the device structure. The bottom layer is composed of c-TiO_2 layers on a glass/FTO substrate acting as electron transporting. Light is absorbed by the Sb_2S_3 layer, while holes are transported by the P3HT HTL and collected at the Au counter electrode.

The Sb_2S_3 absorbing layer was deposited via the FCA using the Sb complex precursor to realize very large grain sizes. The precursor was thermally decomposed to the amorphous state at 200 °C for 1 min and crystalline state at 350 °C for 2 min (Fig. 1b). The SEM image shown in Fig. 2 indicates a very large grain size, which is almost the same as the Sb_2S_3 thin film morphology reported by Wang et al. [22].

The efficiency of the planar-type Sb_2S_3 solar cell was improved via surface treatment with Cs_2CO_3 of the c-TiO_2 layer.

The device properties based on the concentration of Cs_2CO_3 solution were performed to determine the optimum Cs_2CO_3 concentration. Figure 3a and Table 1 show the *J*–*V* characteristics for the devices using different concentrations of Cs_2CO_3 solution under AM 1.5G illumination (100 mW/cm^2). When the concentration is too low (1 mg/mL), there is a problem in whole coverage of the c-TiO_2 surface with Cs_2CO_3. However, if it is too high (5 and 10 mg/mL), it acts as a dielectric material, resulting in an increase in the series resistance and decrease in the device efficiency. The optimum concentration of Cs_2CO_3 was found to be 3 mg/mL. (Hereafter, "with Cs_2CO_3 treatment" means treatment using 3 mg/mL concentration of Cs_2CO_3 unless otherwise noted.)

As a result, the device had a PCE of 2.83%, V_{OC} of 0.549 V, J_{SC} of 10.71 mA/cm^2, and FF of 48.14% before the treatment. However, after the treatment with 3 mg/mL solution, all these parameters increased significantly, i.e., to a V_{OC} of 0.596 V, J_{SC} of 11.71 mA/cm^2, and FF of 56.89%, leading to a PCE of 3.97%. This treatment resulted in a ~ 40% improvement in the PCE. The higher EQE over full spectrum range as shown in Fig. 3b indicates that the light is more efficiently converted into current leading to increase in J_{SC} by this Cs_2CO_3 treatment. From the EQE spectra, we can also see that the onset of EQE at 750 nm corresponds well to a band gap

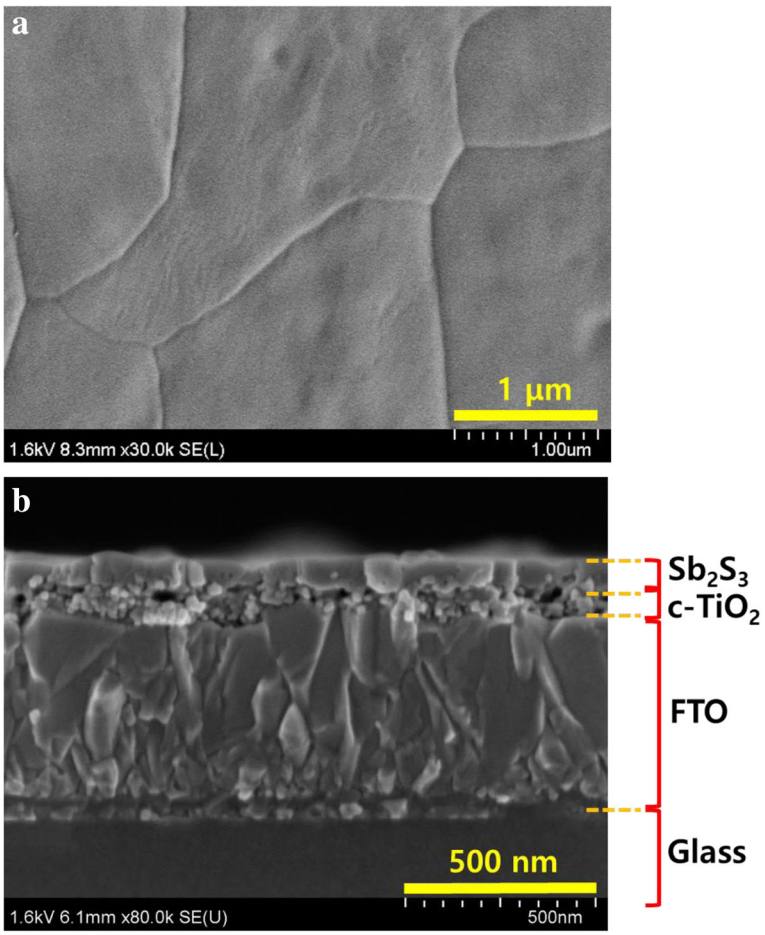

Fig. 2 **a** Top view and **b** cross-sectional SEM images of Sb_2S_3 absorbing layer after annealing at 350 °C for 2 min

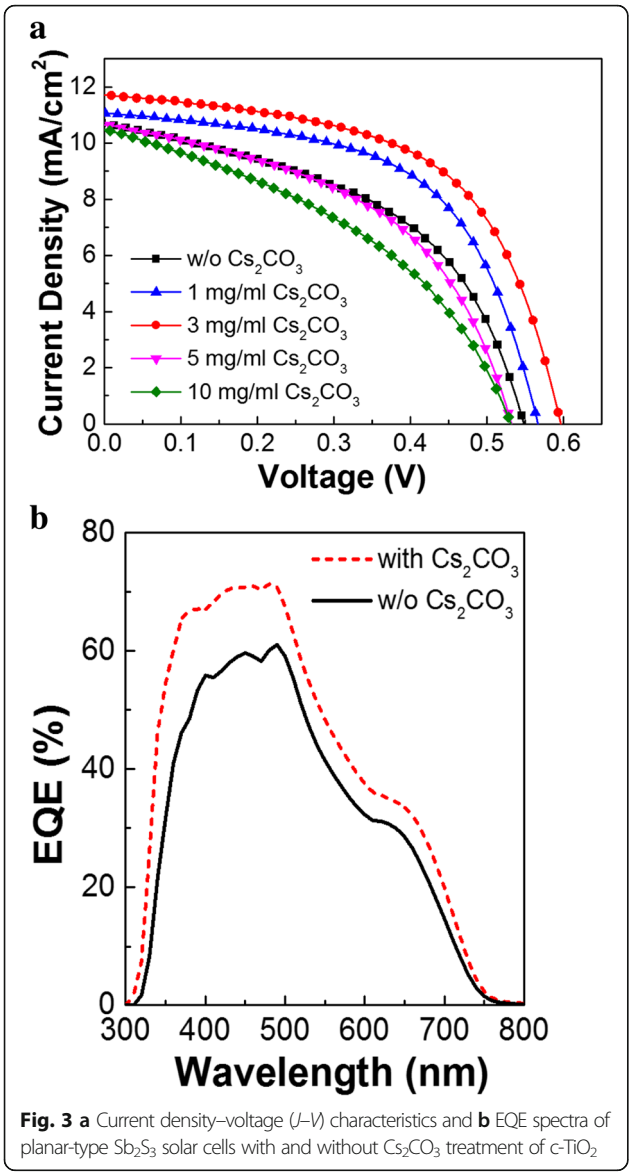

Fig. 3 **a** Current density–voltage (*J*–*V*) characteristics and **b** EQE spectra of planar-type Sb_2S_3 solar cells with and without Cs_2CO_3 treatment of c-TiO_2

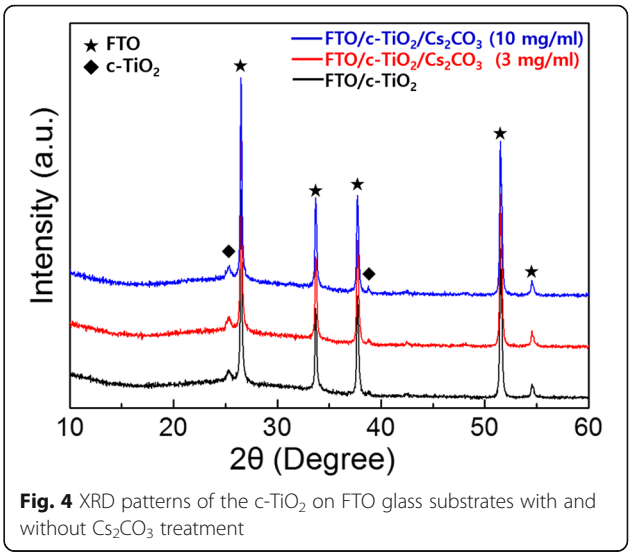

Fig. 4 XRD patterns of the c-TiO_2 on FTO glass substrates with and without Cs_2CO_3 treatment

Table 1 Summary of device performances according to different Cs_2CO_3 concentrations under AM 1.5G condition

Devices	V_{OC} (V)	FF (%)	J_{SC} (mA/cm²)	PCE (%)	R_S (Ω cm²)	R_{SH} (Ω cm²)
Without Cs_2CO_3	0.549	48.14	10.71	2.83	11.14	178.56
With 1 mg/mL Cs_2CO_3	0.567	56.82	11.07	3.56	9.42	451.2
With 3 mg/mL Cs_2CO_3	0.596	56.89	11.71	3.97	8.82	454.08
With 5 mg/mL Cs_2CO_3	0.532	47.99	10.66	2.72	10.66	207.36
With 10 mg/mL Cs_2CO_3	0.531	40.78	10.50	2.27	15.17	125.76

of 1.65 eV for Sb_2S_3 layer and a decrease in EQE from 500 to 650 nm is attributed to the absorption of P3HT HTL layer.

We measured the XRD patterns of the c-TiO_2 on FTO glass substrates with and without Cs_2CO_3 treatment to investigate whether Cs_2CO_3 has effects on the crystallization of the c-TiO_2 layer and/or the formation of new secondary phase by diffused Cs-related species. There was no change in the XRD peak after Cs_2CO_3 treatment as shown in Fig. 4. This indicates that the Cs_2CO_3 treatment has little effect on the crystal structure of c-TiO_2 and also does not create a new phase. Furthermore, there was no evidence of a decomposed Cs-related phase (cesium oxide, cesium suboxide, or Cs element) after thermal treatment of Cs_2CO_3, which means that the thickness of the Cs_2CO_3 is very thin. As shown in Fig. 5d, the thickness of Cs-related species was about 2~3 nm, which was determined by XPS depth profile analysis for the sample of FTO/c-TiO_2/Cs_2CO_3 (3 mg/mL). The measured thickness of Cs_2CO_3 (2~3 nm) is in good agreement with the AFM analysis, which shows improved surface roughness through Cs_2CO_3 treatment from 9.89 to 8.03 nm (see Fig. 6a).

We studied the surface state of the c-TiO_2 layer using XPS measurements. The XPS spectra in Fig. 5 show that both the survey scan and Cs 3d peak scan clearly indicate the existence of Cs on the c-TiO_2 surface. The Ti 2p and O 1 s peaks were shifted to lower binding energies owing to the Cs_2CO_3 treatment, which indicates that the Cs_2CO_3 treatment affected the electronic structure of the c-TiO_2 layer. The appearance of a slight shoulder at ~ 531 eV in the O 1 s spectrum could be attributed to the cesium oxide generated from Cs_2CO_3 decomposition via annealing at 150 °C, which has a low work function [26].

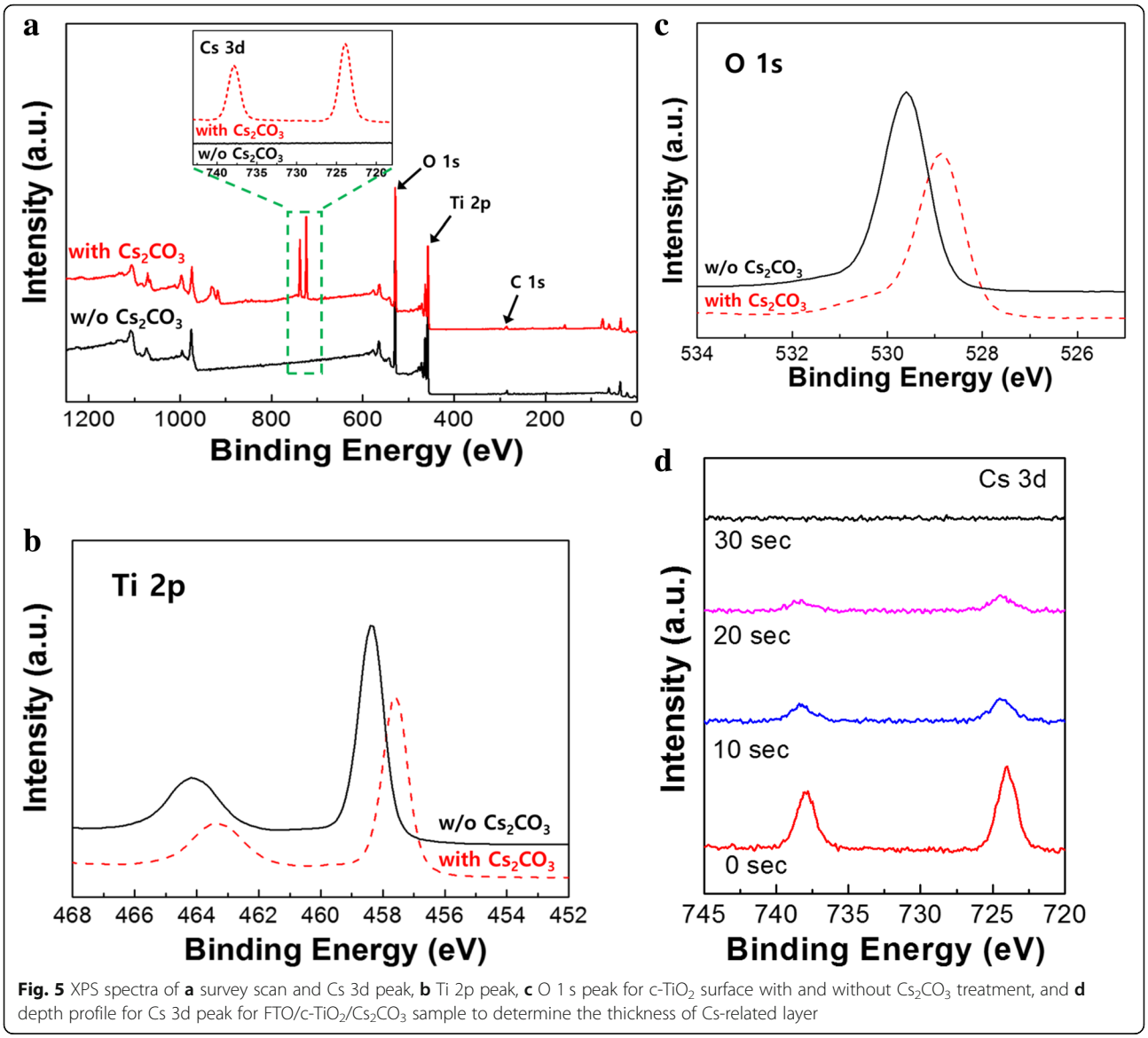

Fig. 5 XPS spectra of **a** survey scan and Cs 3d peak, **b** Ti 2p peak, **c** O 1 s peak for c-TiO_2 surface with and without Cs_2CO_3 treatment, and **d** depth profile for Cs 3d peak for FTO/c-TiO_2/Cs_2CO_3 sample to determine the thickness of Cs-related layer

The AFM images in Fig. 6a reveal a difference in the surface morphology of the c-TiO_2 layer before and after Cs_2CO_3 treatment. The surface became smoother and the root mean square roughness (Rg) decreased from 9.89 to 8.03 nm after treatment. This smooth surface was useful for increasing the physical contact between the c-TiO_2(/Cs_2CO_3) layer and the Sb_2S_3 layer, leading to a decrease in the R_S value from 11.14 Ω cm^2 (without Cs_2CO_3) to 8.82 Ω cm^2 (with Cs_2CO_3) (see Table 1). The decreased R_S may have contributed to increasing the FF from 48.14 to 56.89% [5].

The UV-Vis transmittance spectra of the c-TiO_2 films with and without Cs_2CO_3 are shown in Fig. 6b. The figure shows that there is little change in the optical transmittance between wavelengths of 300 and 800 nm, which confirms that Cs_2CO_3 treatment has a negligible effect on the intensity of light reaching the Sb_2S_3 layer.

UPS was used to determine the change in the work function of the c-TiO_2 layer before and after Cs_2CO_3 treatment to investigate the effect of Cs_2CO_3 on V_{OC}. The results are shown in Fig. 7a. The work function of c-TiO_2 decreases by 0.3 eV after Cs_2CO_3 treatment. Cs_2CO_3 is widely used as an efficient electron transport material in many optoelectronic devices through thermal evaporation or solution process. However, the accurate analysis of electron transport mechanism and the type of decomposed Cs-related species that are responsible for electron transport property are still uncertain and controversial. Among previous reports on solution-processed Cs_2CO_3, Liao et al. showed that Cs_2CO_3 can be decomposed into low work function,

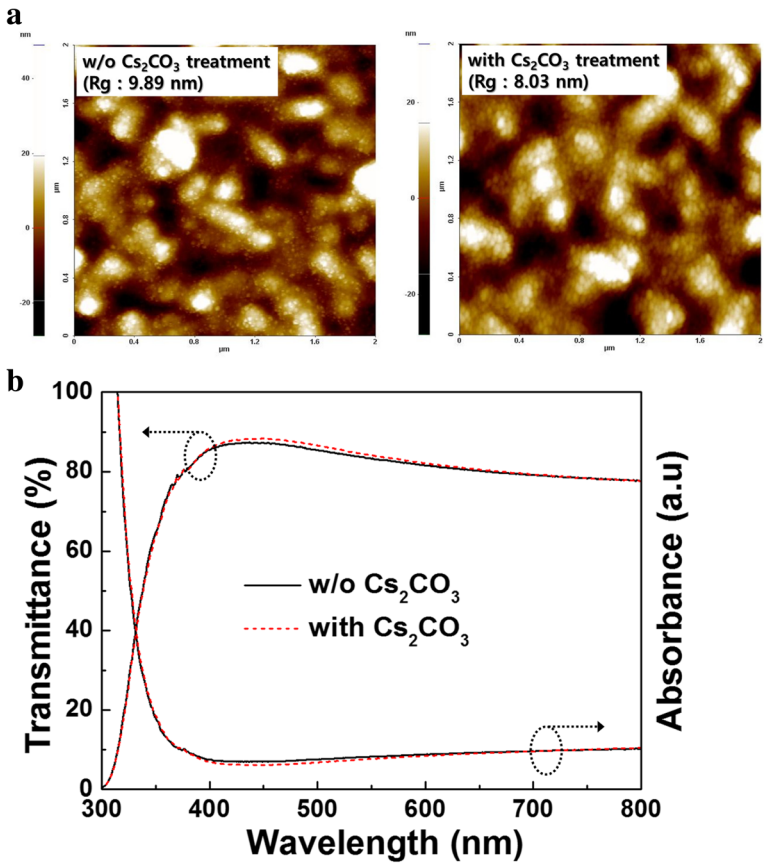

Fig. 6 **a** AFM images (2 μm × 2 μm) of the surface morphology and **b** UV-Vis absorption and transmission spectra of c-TiO_2 with and without Cs_2CO_3 treatment

doped semiconductor in the form of Cs_2O doped with Cs_2O_2 after thermal annealing at 150 °C by using XPS analysis [26]. This form of doped cesium oxide can act as an n-type semiconductor with intrinsically low work function, which might contribute to work function reduction of c-TiO_2 in our system. In addition, there was no change in the absorption onset as shown in Fig. 6b, indicating little change in the optical bandgap of the c-TiO_2 after the treatment.

The energy band diagram in Fig. 7b shows that the conduction band energy level of c-TiO_2 shifted toward a lower energy by 0.3 eV. This shift leads to not only an improved V_{OC} due to an increase in the built-in potential (V_{BI}) inside the devices, but also an increased J_{SC} due to the alignment of the energy level between c-TiO_2 and Sb_2S_3 to reduce the charge transport barrier at the interface. The proposed operating principle is illustrated in Fig. 7c. At open-circuit condition, the shifted conduction band of the c-TiO_2 layer by Cs_2CO_3 treatment leads to the increased V_{BI}, which contributes to the improved V_{OC}. At the same time, the increased V_{BI} results in the larger energy band bending of the Sb_2S_3 layer under short-circuit conditions, and thus the photogenerated electrons can move quickly toward the c-TiO_2 layer. This fast electron transport is attributed to cause the enhanced J_{SC} and FF. Thus, the Cs_2CO_3 treatment on c-TiO_2 layer could increase both V_{OC} and J_{SC} simultaneously, leading to the enhanced PCE. Hence, Cs_2CO_3 is a promising material for c-TiO_2 surface modification as it enhances device performance by changing the work function and improving the electron transport properties.

Conclusions

Cs_2CO_3 was found to be an effective surface modifier to enhance the charge transport ability of the c-TiO_2 electron transport layer (ETL) for planar-type Sb_2S_3 solar cells. The UPS data show that Cs_2CO_3 treatment can shift the work function of c-TiO_2 upward, possibly increasing the built-in potential of the device and reducing the energy barrier for charge transport. The c-TiO_2 surface became smoother after Cs_2CO_3 treatment, resulting in increased physical contact with the

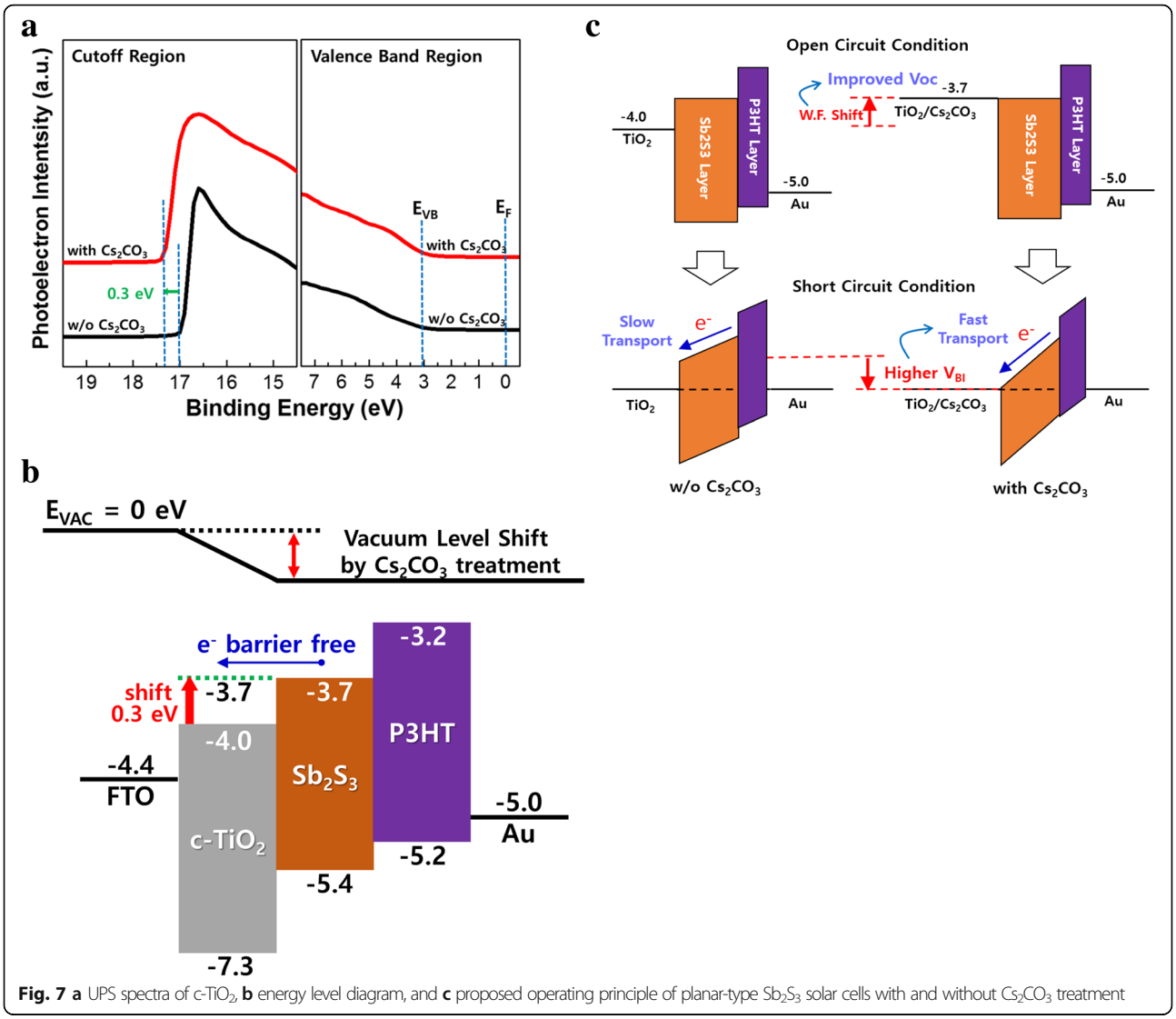

Fig. 7 **a** UPS spectra of c-TiO_2, **b** energy level diagram, and **c** proposed operating principle of planar-type Sb_2S_3 solar cells with and without Cs_2CO_3 treatment

Sb_2S_3 absorber. The solar cell performance was significantly improved in all parameters simultaneously including V_{OC}, J_{SC}, and FF. This resulted in an increase in the PCE from 2.83 to 3.97%, almost a 40% increase. This study shows that surface treatment using inorganic compounds such as Cs_2CO_3 will play an important role in the development of highly efficient planar-type Sb_2S_3 solar cells.

Abbreviations

AFM: Atomic force microscopy; c-TiO_2: Compact TiO_2; EQE: External quantum efficiency; ETLs: Electron transport layers; FCA: Fast chemical approach; FF: Fill factor; FTO: Fluorine-doped tin oxide; HTLs: Hole transport layers; J_{SC}: Short-circuit current density; *J*–*V*: Current density–voltage; m-TiO_2: Mesoporous TiO_2; P3HT: Poly(3-hexylthiophene); PCE: Power conversion efficiency; R_S: Series resistance; R_{SH}: Shunt resistance; SEM: Scanning electron microscopy; UPS: Ultraviolet photoelectron spectroscopy; UV-Vis: Ultraviolet–visible spectrometer; V_{BI}: Built-in potential; V_{OC}: Open-circuit voltage; XPS: X-ray photoelectron spectroscopy; XRD: X-ray diffraction

Acknowledgements

This work was supported by the DGIST R&D Program of the Ministry of Science and ICT of Korea (18-ET-01).

Availability of Data and Materials

All data are available without restriction.

Authors' Contributions

WHK and SW designed the experiments. WHK carried out the experiments. SW prepared the manuscript. WHK and SW performed the main data analysis. KPK, SMK, and DHK participated in the discussion and analysis of the data. All authors read and approved the final manuscript.

Competing Interests

The authors declare that they have no competing interests.

Publisher's Note

Received: 12 October 2018 Accepted: 6 January 2019
Published online: 17 January 2019

References

1. Azimi H, Hou Y, Brabec CJ (2014) Towards low-cost, environmentally friendly printed chalcopyrite and kesterite solar cells. Energy Environ Sci 7:1829–1849
2. Todorov TK, Tang J, Bag S, Gunawan O, Gokmen T, Zhu Y et al (2013) Beyond 11% efficiency: characteristics of state of the art $Cu_2ZnSn(S,Se)_4$ solar cells. Adv Energy Mater 3:34–38
3. Maiti N, Im SH, Lim C-S, Seok SI (2012) A chemical precursor for depositing Sb_2S_3 onto mesoporous TiO_2 layers in nonaqueous media and its application to solar cells. Dalton Trans 41:11569–11572
4. Kamruzzaman M, Chaoping L, Yishu F, Farid UI Islam AKM, Zapien JA (2016) Atmospheric annealing effect on TiO_2/Sb_2S_3/P3HT heterojunction hybrid solar cell performance. RSC Adv 6:99282–99290
5. Lei H, Yang G, Guo Y, Xiong L, Qin P, Dai X et al (2016) Efficient planar Sb_2S_3 solar cells using a low-temperature solution-processed tin oxide electron conductor. Phys Chem Chem Phys 18:16436–16443
6. Choi YC, Lee DU, Noh JH, Kim EK, Seok SI (2014) Highly improved Sb_2S_3 sensitized-inorganic–organic heterojunction solar cells and quantification of traps by deep-level transient spectroscopy. Adv Funct Mater 24:3587–3592
7. Kondrotas R, Chen C, Tang J (2018) Sb_2S_3 solar cells. Joule 2:857–878
8. O'Mahony FTF, Lutz T, Guijarro N, Gómez R, Haque SA (2012) Electron and hole transfer at metal oxide/Sb_2S_3/spiro-OMeTAD heterojunctions. Energy Environ Sci 5:9760–9764
9. Moon S-J, Itzhaik Y, Yum J-H, Zakeeruddin SM, Hodes G, Grätzel M (2010) Sb_2S_3-based mesoscopic solar cell using an organic hole conductor. J Phys Chem Lett 1:1524–1527
10. Boix PP, Larramona G, Jacob A, Delatouche B, Mora-Seró I, Bisquert J (2012) Hole transport and recombination in all-solid Sb_2S_3-sensitized TiO_2 solar cells using CuSCN as hole transporter. J Phys Chem C 116:1579–1587
11. Chang JA, Rhee JH, Im SH, Lee YH, Kim HJ, Seok SI et al (2010) High-performance nanostructured inorganic–organic heterojunction solar cells. Nano Lett 10:2609–2612
12. Im SH, Lim CS, Chang JA, Lee YH, Maiti N, Kim HJ et al (2011) Toward interaction of sensitizer and functional moieties in hole-transporting materials for efficient semiconductor-sensitized solar cells. Nano Lett 11: 4789–4793
13. Tsujimoto K, Nguyen D-C, Ito S, Nishino H, Matsuyoshi H, Konno A et al (2012) TiO_2 surface treatment effects by Mg^{2+}, Ba^{2+}, and Al^{3+} on Sb_2S_3 extremely thin absorber solar cells. J Phys Chem C 116:13465–13471
14. Lan C, Luo J, Lan H, Fan B, Peng H, Zhao J et al (2018) Enhanced charge extraction of Li-doped TiO_2 for efficient thermal-evaporated Sb_2S_3 thin film solar cells. Materials 11:355
15. Fukumoto T, Moehl T, Niwa Y, Nazeeruddin Md K, Grätzel M, Etgar L (2013) Effect of interfacial engineering in solid-state nanostructured Sb_2S_3 heterojunction solar cells. Adv Energy Mater 3:29–33
16. Savadogo O, Mandal KC (1994) Low cost Schottky barrier solar cells fabricated on CdSe and Sb_2S_3 films chemically deposited with silicotungstic acid. J Electrochem Soc 141:2871–2877
17. Escorcia-García J, Becerra D, Nair MTS, Nair PK (2014) Heterojunction CdS/Sb_2S_3 solar cells using antimony sulfide thin films prepared by thermal evaporation. Thin Solid Films 569:28–34
18. Yuan S, Deng H, Dong D, Yang X, Qiao K, Hu C et al (2016) Efficient planar antimony sulfide thin film photovoltaics with large grain and preferential growth. Sol Energy Mater Sol Cells 157:887–893
19. Yuan S, Deng H, Yang X, Hu C, Khan J, Ye W et al (2017) Postsurface selenization for high performance Sb_2S_3 planar thin film solar cells. ACS Photonics 4:2862–2–70
20. Kim D-H, Lee S-J, Park MS, Kang J-K, Heo JH, Im SH et al (2014) Highly reproducible planar Sb_2S_3-sensitized solar cells based on atomic layer deposition. Nanoscale 6:14549–14554
21. Wang W, Strössner F, Zimmermann E, Schmidt-Mende L (2017) Hybrid solar cells from Sb_2S_3 nanoparticle ink. Sol Energy Mater Sol Cells 172:335–340
22. Wang X, Li J, Liu W, Yang S, Zhu C, Chen T (2017) A fast chemical approach towards Sb_2S_3 film with a large grain size for high-performance planar heterojunction solar cells. Nanoscale 9:3386–3390
23. Wang G, Wang S, Cui Y, Pan D (2012) A novel and versatile strategy to prepare metal–organic molecular precursor solutions and its application in $Cu(In,Ga)(S,Se)_2$ solar cells. Chem Mater 24:3993–3997
24. Zimmermann E, Pfadler T, Kalb J, Dorman JA, Sommer D, Hahn G et al (2015) Toward high-efficiency solution-processed planar heterojunction Sb_2S_3 solar cells. Adv Sci 2:1500059
25. Sung S-J, Gil EK, Lee S-J, Choi YC, Yang K-J, Kang J-K et al (2017) Systematic control of nanostructured interfaces of planar Sb_2S_3 solar cells by simple spin-coating process and its effect on photovoltaic properties. J Ind Eng Chem 56:196–202
26. Liao H-H, Chen L-M, Xu Z, Li G, Yang Y (2008) Highly efficient inverted polymer solar cell by low temperature annealing of Cs_2CO_3 interlayer. Appl Phys Lett 92:173303
27. Chen F-C, Wu J-L, Yang SS, Hsieh K-H, Chen W-C (2008) Cesium carbonate as a functional interlayer for polymer photovoltaic devices. J Appl Phys 103: 103721
28. Kim HP, bin Mohd Yusoff AR, Lee HJ, Lee SJ, Kim HM, Seo GJ et al (2014) Effect of ZnO:Cs_2CO_3 on the performance of organic photovoltaics. Nanoscale Res Lett 9:323
29. Li Y, Zhang D-Q, Duan L, Zhang R, Wang L-D, Qiu Y (2007) Elucidation of the electron injection mechanism of evaporated cesium carbonate cathode interlayer for organic light-emitting diodes. Appl Phys Lett 90:012119
30. Qin L, Xie Z, Yao L, Yan Y, Pang S, Wei F et al (2014) Enhancing the efficiency of TiO_2–perovskite heterojunction solar cell via evaporating Cs_2CO_3 on TiO_2. Phys Status Solidi RRL 8:912–916
31. Dong H, Guo X, Li W, Wang L (2014) Cesium carbonate as a surface modification material for organic–inorganic hybrid perovskite solar cells with enhanced performance. RSC Adv 4:60131–60134